Chapter 6
A Custom Instrument for Electromechanical Characterization

This chapter deals with the development of an instrument for electromechanical characterization of fabricated devices. Precise electromechanical characterization of micromachined structures is of great relevance for several reasons. It represents an experimental validation of theory, behavioral simulations [1] and FEM models [2] of devices; it allows to improve and refine these models through a comparison with experimental data; it enables the estimation of unknown mechanical parameters (for instance, the damping coefficient when packaging conditions are not completely known [3]; or the overetch/underetch with respect to the design layout; or mechanical offsets due to residual stresses); it allows to compute equivalent electrical LCR models for Micro- and Nano-Electromechanical Systems (M/NEMS) resonators [4]; finally, it is a step for testing devices on the industrial scale, to check their yield, reproducibility [5], aging [6], and reliability [7].

Section 6.2 describes working principle, design, and main features of this characterization instrument. This platform is implemented on a PCB with discrete components and then calibrated. Chapter 7 reports electrical measures performed on magnetometers with the developed instrument.

6.1 Motivations for a Custom Instrument

The instrumentation available on the market for electromechanical characterization includes (1) semiconductor parameter analyzers and (2) optical instrumentation for in-plane and/or out-of-plane monitoring of the position of the device suspended structure. The former is basically represented by capacitance meters: these instruments generally have a good (sub-fF) resolution, but they do not allow the dynamic device characterization as their measurement bandwidth is limited. As an example, the *Agilent E4980A Precision LCR meter* [8] provides, at an integration time of $\approx$30 ms (corresponding to $\approx$33 Hz), a maximum fluctuation in the capacitance

C. Buffa, *MEMS Lorentz Force Magnetometers*,
DOI 10.1007/978-3-319-59412-5_6

measurements of 0.5 fF (at 20 mV of test signal amplitude). Similar performance can be obtained using the *QuadTech 7600 Plus Precision LCR Meter* [9]. Optical instrumentation (laser-Doppler and vibrometers) can be used for a full mechanical characterization of MEMS (e.g., the *Polytec PMA-400 Planar Motion Analyzer* [10] has a measurement bandwidth up to 1 MHz). However these instruments require precise optical alignment, stroboscopic cameras, high speed imagers, etc. and are thus very costly (about ten times the electrical ones). Besides, they have a major limit in that they do not allow the analysis of packaged devices: this is a crucial issue, as M/NEMS devices behavior and reliability strongly depend on the packaging conditions[1] (in fact, a measurement at atmosphere pressure does not describe the dynamic behavior of the packaged device). Other examples of research efforts to develop versatile instrumentation for the visual analysis of MEMS devices can be found in [11, 12].

There is no electrical instrument specifically designed for M/NEMS characterization on the market. In this section is presented a prototype of a Mechanical Characterization Platform (MCP), whose aim is filling this lack by providing a complete mechanical characterization for designed magnetometers and, more in general, a lot of capacitive M/NEMS devices. The MCP is intended to be as more versatile as possible because capacitive M/NEMS sensors can differ in terms of process (minimum dimensions, air gap), geometry (characteristic frequency, pull-in voltage), operation (quasi-stationary or resonant), and packaging. The MCP is formed by different elements:

- a differential driving PCB electronic board that is used for capacitive actuation;
- a custom developed, lock-in type, readout PCB electronic board for low-noise and high-sensitivity real-time monitoring of the capacitance variation of the M/NEMS and its conversion into a voltage signal;
- a socket to host either the M/NEMS chip or standard industrial coaxial connectors for wafer-level probe testing;
- a Data Acquisition Board (DAQ) interconnecting the driving/readout PCB to a workstation;
- LabVIEW (by National Instruments™) software libraries for tests automation.

The platform exploits different kinds of electrical stimuli and monitors the resulting capacitance variation, via real-time capacitive sensing. The measurement types are stationary (C-V curves) and dynamic (responses to input steps in the time domain). The data can then be converted into Bode plots in the frequency domain. Experimental results show that the MCP measurement resolution approaches 1 aF/$\sqrt{\text{Hz}}$, with a temperature drift lower than 100 ppm/°C. The sensing of the capacitance variation is based on a small-amplitude voltage test signal with a frequency of 1 MHz, which restricts the bandwidth range of measurable devices to approximately 100 kHz, as will be detailed in the following section.

[1] Some devices are designed to work at ambient pressure. Nevertheless, in most times a cap on top of device is required to prevent from damages.

6.2 System Overview

The MCP prototype is constituted by a driving/sensing electronic PCB motherboard, a data acquisition board, and software for data processing and displaying. If the wafer is diced, the M/NEMS device can be wire bonded to a standard ceramic carrier or to a small PCB socket that are then connected to the motherboard. Alternatively, the M/NEMS can be on-wafer (wafer is not diced) and a different PCB socket, with coaxial-type connectors, is used for electrical connections between the probe station where the wafer is held and the MCP. A block scheme of the MCP is given in Fig. 6.1. The user selects the input parameters (type of analysis, input waveform, number of averages, etc.) on a LabVIEW interface. Through GPIB connections, the software controls a voltage source that provides the desired stimulus. The software is also connected and synchronized with the readout PCB. More details on the different blocks are given below.

It is now considered a generic M/NEMS capacitive device which includes a differential driving and a differential sensing configuration (see Fig. 6.2), with a suspended structure forming two pairs of capacitances ($C_{d,i}(t)$ and $C_{s,i}(t)$, respectively) with the fixed stators. Capacitances can be of the parallel-plate type (as in the figure), of the comb-finger type or based on fringe effects [13].

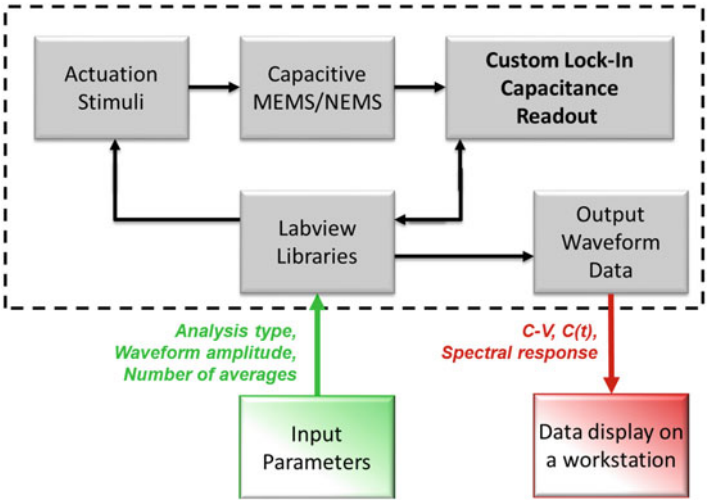

Fig. 6.1 Block-scheme illustration of the Mechanical Characterization Platform. The user can choose the type of measurements and other options (amplitude, averages, initial offset, resolution, etc.) and visualize the results through a LabVIEW interface

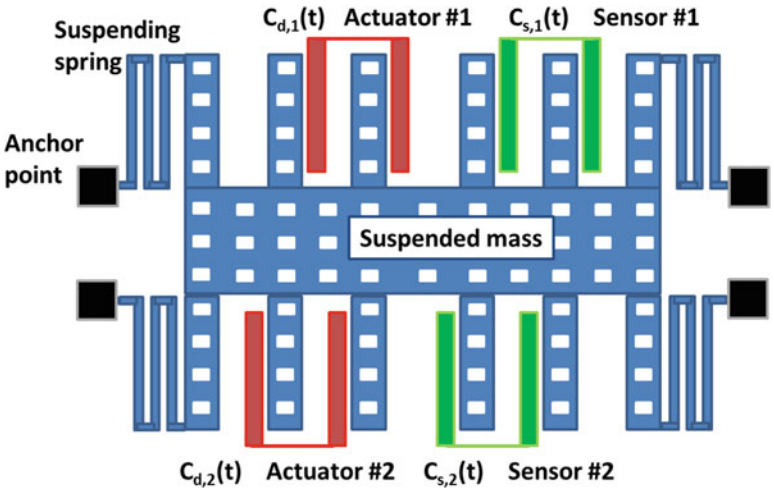

Fig. 6.2 Simplified model of a generic differential-drive, differential-sense, capacitive M/NEMS device

6.2.1 Driving Electronics

Electrostatic driving elements are often part of a M/NEMS device. For some sensors, like gyroscopes, magnetometers or resonant devices [14, 15], driving is always necessary during the device operation. In other situations, like in accelerometers, microphones and pressure sensors driving is not necessary during operation but it may be useful for an initial calibration procedure [16]. For test structures designed to study specific material properties or reliability (e.g. fracture or fatigue tests) driving is mandatory and it is much simpler to embed an electrostatic actuation on-chip rather than using an out-of-chip generated force.

These actuators, often present in the device layout, can be conveniently used to apply electrostatic test stimuli for the device characterization.

In order to make the driving stage of the MCP as more versatile as possible, a differential actuation scheme has been implemented. This scheme gives the possibility to simultaneously apply electrostatic loads in different directions, or to combine the application of both tensile and compressive stresses to a device for reliability tests (the importance of having such a type of actuation is motivated for instance, by the strong dependence of fatigue reliability of polysilicon micro and nano structure on the ratio between the compressive and the tensile stresses during fatigue cycles) [7].

The schematic of the driving stage is represented in Fig. 6.3. Considering a generic periodic input voltage $v_d(t) = A \cdot \mathscr{F}(2\pi \cdot f_d \cdot t)$ provided by an external source (a voltage supply or a waveform generator), where $\mathscr{F}$ is a generic periodic function and A is its amplitude, two output signals are fed to the two M/NEMS driving electrodes:

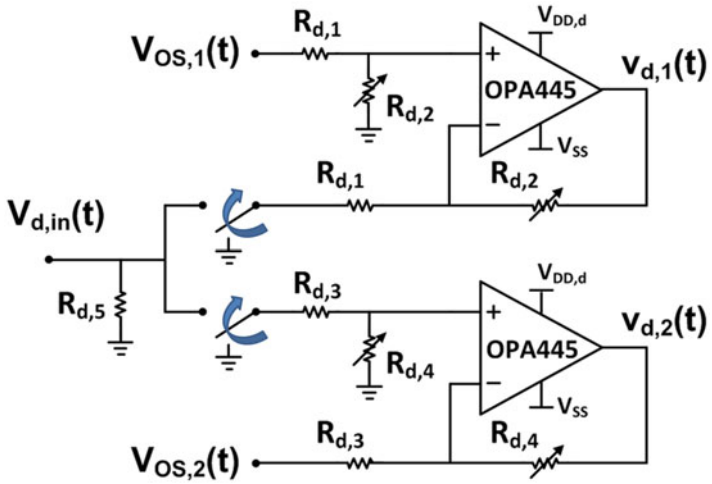

Fig. 6.3 Electronic schematic of the driving stage: two amplifiers generate amplified output signals with a 180° phase difference. The gain and offset of the signals can be selected through the trimming resistors

$$v_{d,1}(t) = V_{\mathrm{OS}_1} \cdot \frac{R_{d,2}}{R_{d,1}} + v_{d,\mathrm{in}} \cdot \frac{R_{d,2}}{R_{d,1}} \cdot \mathscr{F}(2 \cdot \pi f_d \cdot t + \pi) \,, \tag{6.1}$$

$$v_{d,2}(t) = -V_{\mathrm{OS}_2} \cdot \frac{R_{d,4}}{R_{d,3}} + v_{d,\mathrm{in}} \cdot \frac{R_{d,4}}{R_{d,3}} \cdot \mathscr{F}(2 \cdot \pi f_d \cdot t) \,, \tag{6.2}$$

where $\frac{R_{d,2}}{R_{d,1}}$ and $\frac{R_{d,4}}{R_{d,3}}$ are voltage amplification of the two difference amplifiers and can be set using potentiometers ($R_{d,2}, R_{d,4}$) and V_{OS_i} are offset coefficients, again selectable through trimming resistors (not shown in this simplified schematic). Alternatively, offset voltages can be supplied using an analog output board controlled by LabVIEW software. The driving interface can be clearly used as single ended, either on actuation side 1 or on side 2, by suitably zeroing one of the potentiometers. The selected operational amplifier for these stages is the *OPA445* by *Texas Instruments*, capable of standing up to 90 V of differential voltage supply with a good temperature immunity (typical offset drift $\approx$25 μV/°C) and a fast slew rate (15 V/μs). Such a large voltage supply range allows the test of very different kinds of devices. A fast slew rate is also required when it is required to apply large step or impulse voltages to the device (these stimuli are not instantaneous as in the ideal situation: yet they should be much faster than the M/NEMS mechanical bandwidth to be measured). Two switches allow to apply an offset voltage only (with no sine stimulus) at one side, while the sine stimulus is still applied at the other side.

The driving stimuli, so far supplied by external instrumentation, can be replaced in future version by monolithic function generators (discrete electronic components that provide waveform generation with the needed accuracy and versatility) or by direct digital synthesizer (DDS).

6.2.2 Capacitive Readout Electronics

The readout electronics developed for the MCP is biased using a ±5 V voltage source. Its description will be given by highlighting point by point its relevant features:

- *low perturbation of the device*: it is extremely important that during the electromechanical characterization the device behavior is not affected by unwanted electrostatic readout forces. For some capacitive configurations (comb fingers) the effect of the application of a readout electrical signal (a DC or a rapidly varying voltage) is a constant force, independent of the device position. For other configurations (parallel-plate capacitances) the readout force is dependent on the position of the suspended mass and can cause the well-known pull-in instability [17], thus determining the impossibility to test the device. As parallel-plate capacitance sensors have a better sensitivity to area ratio than comb fingers, they are generally adopted for industrial sensors and it thus becomes extremely relevant the development of a low perturbation readout electronics. A further advantage is that, through this approach, also the effect of fringe electrostatic forces, not easily predictable, can be minimized.

  Instead of using a *constant voltage readout* (i.e., with a fixed potential difference applied between the suspended mass contact and the sensing contact) [18], in the proposed MCP the readout signal is obtained from a fast voltage sine wave applied at the suspended mass contact, with each of the sensing electrode kept at virtual ground:

$$v_s(t) = v_0 \cdot \sin(2\pi f_0 \cdot t) \; . \tag{6.3}$$

  The signal is provided by an external waveform generator; in principle, the choice of the amplitude v_0 determines a compromise between the required resolution and the unwanted perturbation (the higher v_0, the larger the sensitivity; the lower v_0, the lower the unwanted readout forces).
- *high sensitivity*: to solve the said compromise and maintain a high sensitivity while keeping a low perturbation, the frequency of the test signal, f_0, must be kept as high as possible. Indeed the current flowing through each sensing capacitance $C_{s,i}$ and into each readout stage, caused by the test signal is:

$$i_{s,i}(t) = C_{s,i} \cdot \frac{dv_s(t)}{dt} + v_s \frac{dC_{s,i}(t)}{dt} \; . \tag{6.4}$$

The second term in the equation above is proportional to the derivative of the capacitance. In quasi-stationary measurements this term is thus null. In dynamic measurements the capacitance change occurs at a maximum frequency equal to the M/NEMS bandwidth f_r. The first term in the equation above is instead proportional to the test frequency f_0. By setting a high $f_0 >> f_r$ a double result is obtained: (1) the current can be simplified as:

$$\begin{aligned} i_{s,i}(t) &= C_{s,i}(t) \cdot \frac{dv_s(t)}{dt} \\ &= C_{s,i}(t) \cdot 2\pi \cdot f_0 \cdot v_0 \cdot \cos(2\pi \cdot f_0 \cdot t) \ , \end{aligned} \tag{6.5}$$

and (2) the current is thus proportional both to the test signal amplitude v_0 and to the test signal frequency f_0, so that the sensitivity can be kept high, even when the amplitude v_0 needs to be low (for the issues described above), by holding a frequency f_0 as high as possible. The same readout principle is adopted in capacitance meters, where the best resolution is obtained at the highest frequency of the stimulus signal.

In the present version of the MCP f_0 can be set up to 1 MHz. This value limits the bandwidth of maximum testable devices to M/NEMS having a bandwidth $f_r < 100$ kHz. The test signal is so far provided by an external waveform generator but it can be replaced by a discrete oscillator, with the required characteristics.

Figure 6.4 shows one channel of the front end electronics, which has now been doubled with respect to the work presented in [19]. This allows a simultaneous differential measurement, an often adopted solution to increase device sensitivity, linearity, and immunity to temperature or other common mode variations. Differential operation is not possible using standard capacitance meters.

The current $i_{s,i}(t)$ of the ith channel flows into the virtual ground of the transimpedance amplifier, ($R_F = 4.75$ kΩ, $C_F = 47$ pF), designed using Analog Devices *OP*42, a fast precision JFET-input operational amplifier with negligible

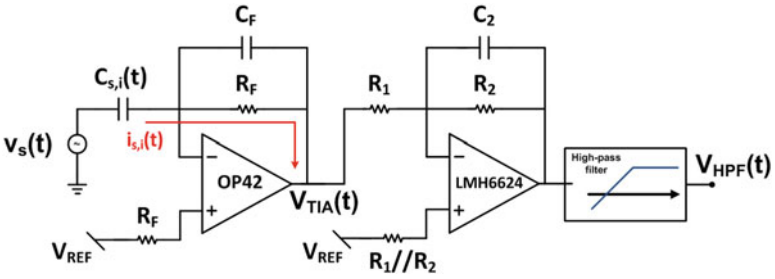

Fig. 6.4 The current flowing in M/NEMS device under test is sensed using a low-noise, low input current and high speed transresistance amplifier. A second gain stage ($G_2 = 47$) is then used to amplify signal to fully exploit demodulation circuit and DAQ board input range. Finally an LC high-pass filter is used to avoid any offset at demodulator inputs

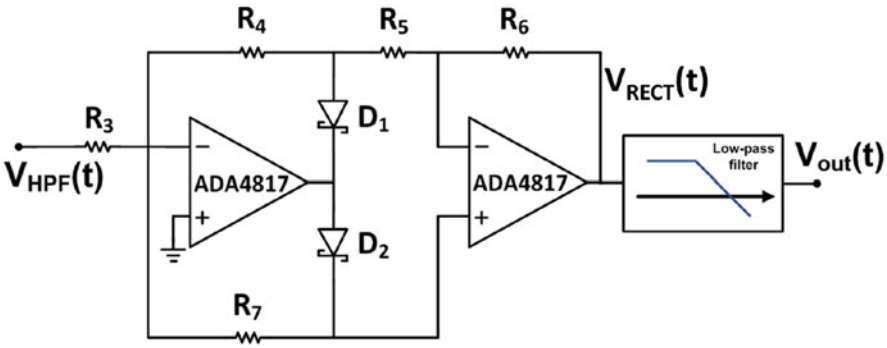

Fig. 6.5 Demodulation is performed through a full-wave diode rectifier: $R_3 = 300\,\Omega$, $R_4 = R_5 = R_6 = 3\,\text{k}\Omega$, and $G = 10$. Fast- and low-noise operational amplifiers combined with Infineon *BAT*62 Schottky diodes are chosen to achieve high frequency demodulation. A closed-loop implementation of the rectifier allows to minimize errors due to turn-on and turn-off diodes time by a factor approximately equal to loop gain

input current noise. The resulting voltage, $v_{\text{TIA}}(t)$ is further amplified by a gain stage based on National Semiconductor *LMH*6624. Input bias current of both stages is compensated with resistors placed at non-inverting input of operational amplifiers. A noiseless second order high-pass filter is then used to filter low-frequency noise and offset which can affect the following demodulating circuit.

- *high resolution*: low-noise readout is required as the capacitance variations to be sensed in miniaturized devices are going into the deep sub-fF range. This is accomplished in the MCP through the use of a custom developed lock-in type detection technique. As the information on the capacitance to be measured is carried by a modulated signal in the MHz range, the low-frequency electronic noise (mainly the $1/f$ contribution of the first operational amplifier) can be filtered at this point to improve the signal to noise ratio (SNR). Considering that $1/f$ noise of CMOS based operational amplifiers has a typical corner frequency around 1 kHz, high-pass filtering at 10–100 kHz is a good choice to erase noise and save signals that are centered around 1 MHz.

  The schematic of the demodulation stage is shown in Fig. 6.5: after filtering, the signal $v_{\text{HPF}}(t)$ is rectified. With respect to previous works by the authors [19], rectifying is now performed using an active diode configuration. Two main advantages of this wholly analog approach are that (1) the need for synchronization signals is eliminated and (2) switching noise and, more in general noise due to digital circuits, is eliminated avoiding cross talk on analog amplifiers. Schottky diodes (D_1 and D_2) are preferred because of their faster turn-on and turn-off times which, combined with a closed-loop solution, are through and through negligible. The rectified output envelope has now the shape of the capacitance variation, so that a low pass filtering at a frequency slightly larger than the M/NEMS resonance frequency gives a demodulated output voltage signal which exactly represents the capacitance variation, in a real-time mode.

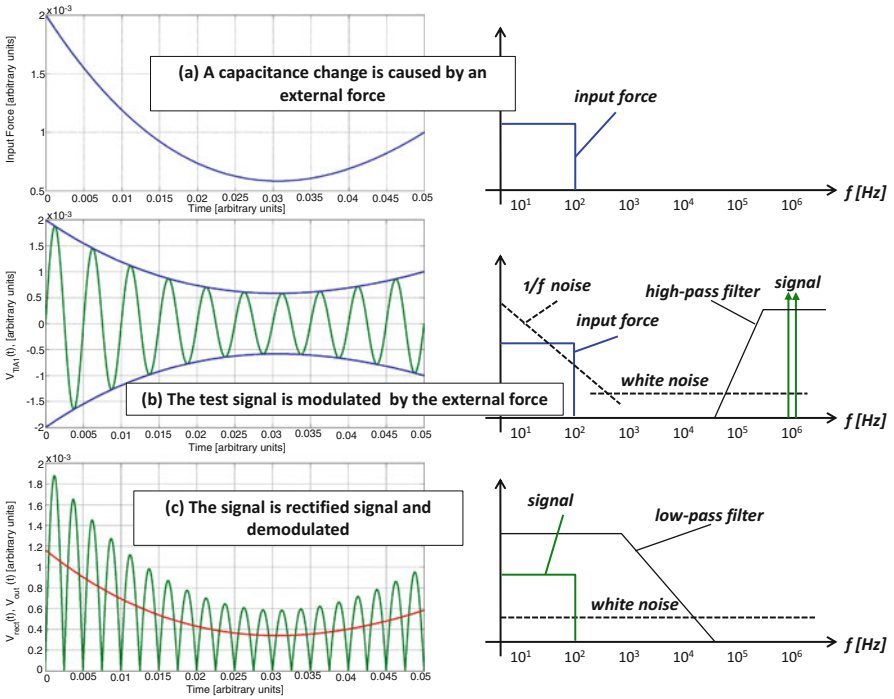

Fig. 6.6 Summary of signals. (**a**) Capacitance rest values change in presence of an acceleration, magnetic field or other forces to be transduced; in the frequency domain input force has a spectrum generally limited to few tens of kHz. (**b**) The application of a high-frequency carrier is fundamental to optimize signals filtering; M/NEMS capacitance variations modulate this high-frequency carriers. (**c**) A low-pass filter (LPF) is required to shift devices signals back to baseband

A set of two different low-pass output filters (selectable by the user through mechanical switches) is provided for each channel.

Figure 6.6b, c summarizes the signals along the MCP readout circuit: in the event of a time varying external force (as in Fig. 6.6a) the sine wave at the output of the transimpedance stage is modulated in amplitude due to the capacitance change, caused by this force. The signal is then rectified and low-pass filtered so that the voltage at the output of the MCP has the same shape as the capacitance change. The representation of the signals in the frequency domain schematically shows the filtering of the low-frequency electronic noise.

6.2.3 *Data Acquisition and Display*

In order to visualize and process the output data and to control all the measurements from the driving to the display of results, two LabVIEW libraries have been developed. One is provided for stationary, the other for dynamic analyses.

In the stationary C-V characterization the LabVIEW program controls via GPIB a DC voltage source (Agilent E3631A) that is swept between two selectable values. The number of steps and thus their amplitude can be also set by the user through the LabVIEW interface. Each time after the driving voltage is changed, the output voltage of the MCP is sampled through a data acquisition board (DAQ PCI4020) and averaged over a selectable number of samples to further increase the resolution. After that the program sets the new voltage value and the procedure is repeated until the last voltage value is reached. This operation is analogous to the measurement procedure of a capacitance meter. However the operation of such an instrument is limited to quasi-stationary analyses, while the proposed MCP can go beyond.

In the dynamic characterization the device is led to a perturbed position (the corresponding voltage is selected by the user) through a quasi-stationary ramp; then the voltage is instantaneously set to zero. The LabVIEW program, which governs all the measurement, is synchronized with the driving voltage and captures the device capacitance variation after the downward step. Due to the low perturbation of the readout electronics, this corresponds to the device free oscillation. Also in this case the user is allowed to select the number of times the measure is repeated in order to further increase the signal to noise ratio by averaging. Such measurements cannot be done by capacitance meters as their bandwidth is limited. Anyway, the user is free to choose among all standard waveforms or specify arbitrary waveforms according to the proper stimulus required by the device under test.

The user interface of the described acquisitions is reported in Fig. 6.7. For all the measurements the data are also saved as text files, expressed in terms of capacitance variation and applied voltage. By fitting the experimental data or by numerically applying a Fourier Transform to the downward step response, the mechanical parameters of the device and its Bode representation can be extrapolated. This will be shown in detail with an example in Sect. 7.1.1.

Figure 6.8a, b shows the connection to the MCP of wafer-level and single MEMS devices, respectively. Shown in Fig. 6.8c is a differential driving, differential sensing MCP, implemented using a 6-layer technology board whose dimensions are $18.3 \times 8\ \text{cm}^2$.

6.3 Board Characterization: Noise and Sensitivity

The MCP has been characterized using the HP4195A Spectrum Analyzer. The transfer function from the input test signal $v_s(t)$ to the voltage at the output of the high-pass filter $v_{\text{HPF}}(t)$ has been measured by connecting the test signal of

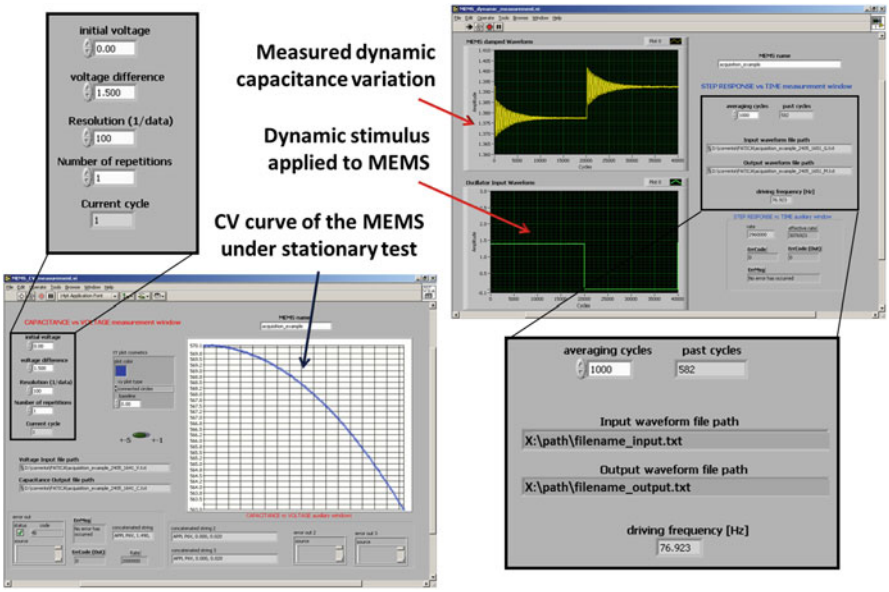

Fig. 6.7 User interface of the static (*left*) and dynamic (*right*) LabVIEW acquisition programs

the analyzer to the input of the MCP, where a 1.02 pF test capacitance (previously measured with the *HP*4274 *LCR* meter) was placed instead of the MEMS sensing capacitance, for correct initial calibration. The test signal had an amplitude $v_0 =$ 450 mV and the frequency swept in the range 10 kHz–10 MHz. Figure 6.9 reports the transfer function measured for the two channels (circle and square markers), compared to the one obtained from *OrCAD Capture* simulations using all the models of the electronic components used in the realized circuit (solid curve). The effect of the high-pass filter in eliminating the low-noise contributions is evident. The transfer function peak occurs around 1 MHz, where the test signal frequency will be conveniently set during the platform operation. The electronic noise was then measured by leaving open the negative input of the transimpedance amplifier while the spectrum analyzer measured the voltage at the output of the MCP, after the low pass filter. For each channel the measurements were repeated for both the low pass filters configurations (10 and 100 kHz). A noise spectral density around 800 $\frac{\text{nV}}{\sqrt{\text{Hz}}}$ is measured (see Fig. 6.10), corresponding to $\approx$1 aF/$\sqrt{\text{Hz}}$ at $v_0 = 450$ mV (measurements are quite disturbed by the proximity to the resolution of the analyzer itself). Using a lower test signal amplitude the unwanted readout force on the device becomes quadratically smaller but, as a drawback, the MCP resolution linearly worsen.

Finally the linearity of the MCP with respect to both the test signal amplitude and the value of the capacitance under measurement was verified, using test capacitances of carefully measured values. First, the parasitic capacitance between

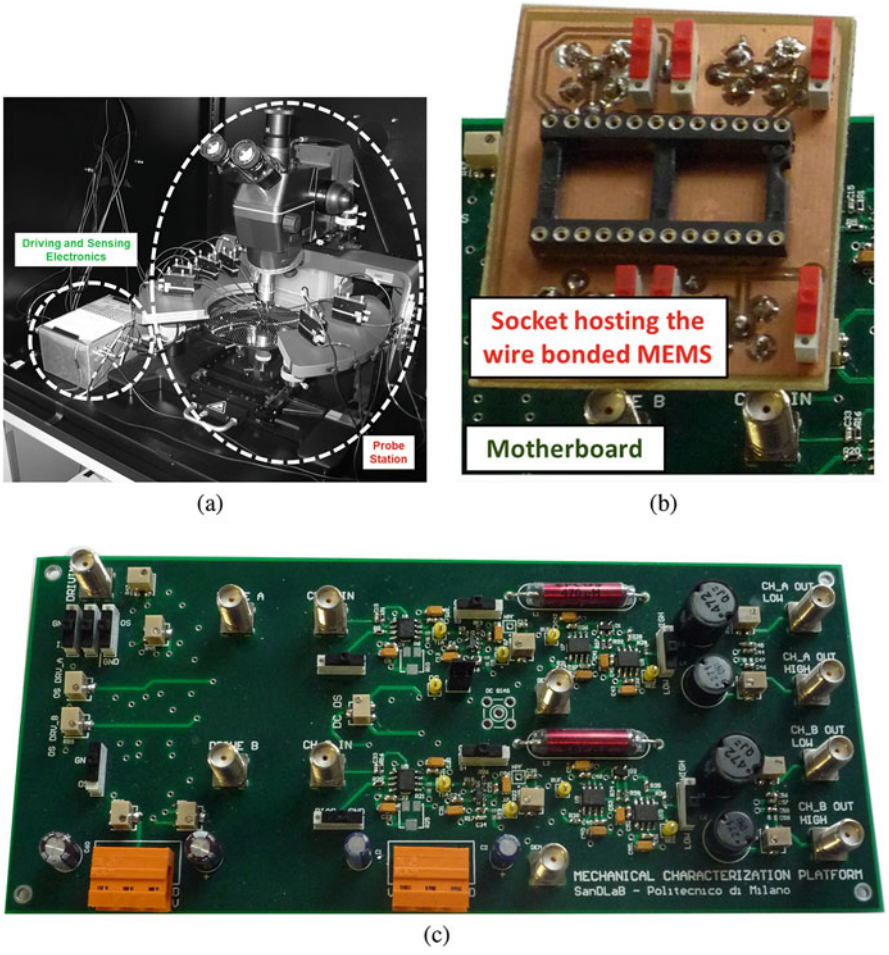

Fig. 6.8 (**a**) View of the MCP box connected to a probe station for wafer-level measurements. Two power supplies are externally connected. (**b**) Close-up view of the socket for diced MEMS measurements. This socket can be plugged in and out of the motherboard. (**c**) Photograph of a final implementation of prototype motherboard using a 6-layer technology

the two socket plugs, connected to the M/NEMS sensing element and the suspended mass respectively, was evaluated. This parasitic has a value around 435 fF. Other parasitic capacitances to ground do not disturb the measure, as they are kept between fixed voltages (true ground and virtual ground). They do not even afflict the stability of the transimpedance stage as far as their value is lower than about a hundred of pF. The rms value of the filtered output voltage was measured in four different conditions of the input test signal v_0 (100, 200, 500, 900 mV_{PP}), for five different capacitances C_s (195, 259, 468, 1282, 2455 fF—values calibrated using the *HP*4274 LCR meter). Figure 6.11 reports these experimental results, which take

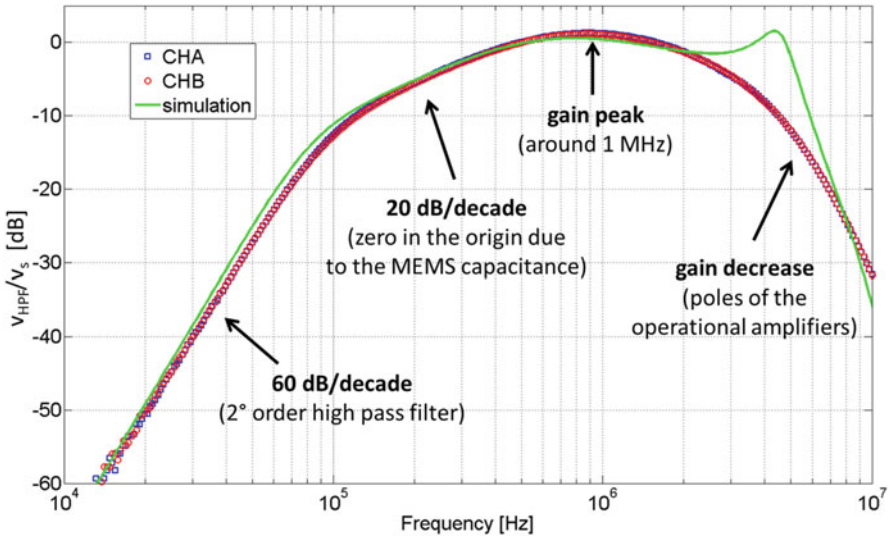

Fig. 6.9 Sensitivity of analog front end of MCP instrument with a test capacitance of 1.02 pF. This transfer function is measured applying a test signal to a test capacitance and reading the resulting voltage at the output of HPF. In the operating region of the MCP (100 kHz and 1 MHz) experimental data fit simulations almost perfectly

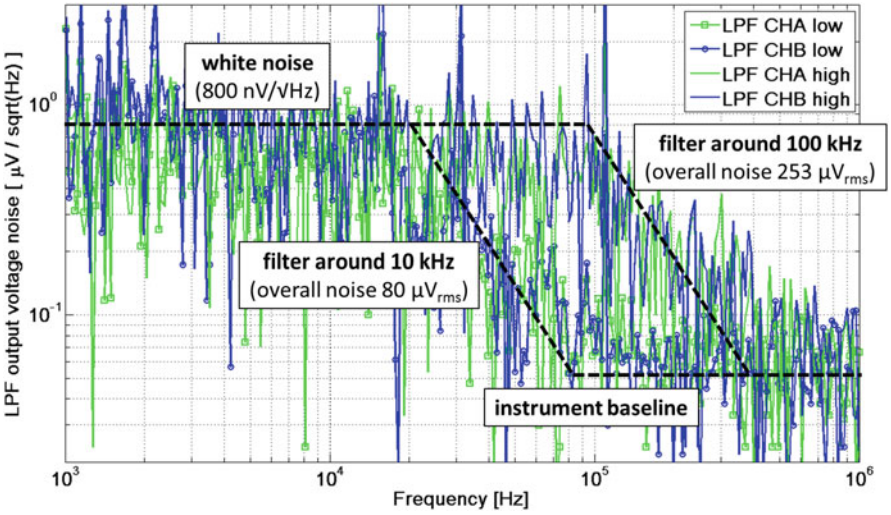

Fig. 6.10 Noise is measured at the output of each channel using HP4195A Spectrum Analyzer

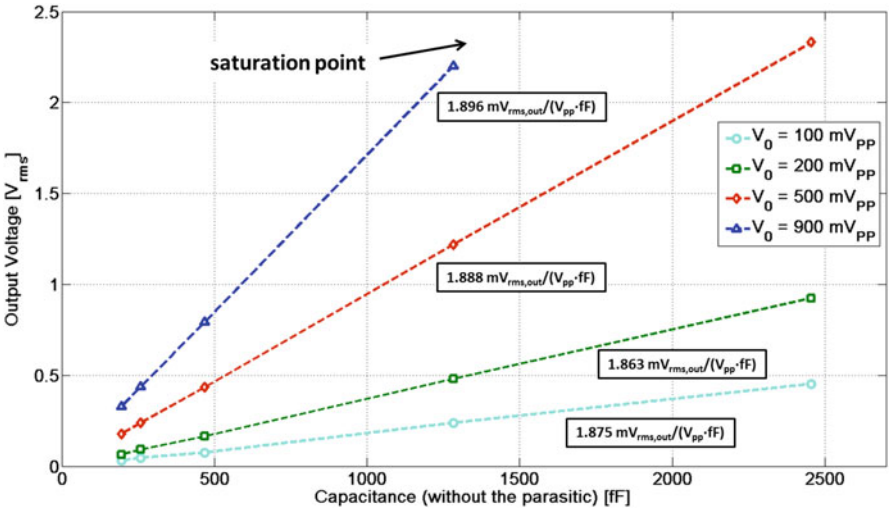

Fig. 6.11 Linearity performance of the presented MCP: measurements are done on a set of four previously calibrated capacitances at four different test signal levels. The evaluated relative linearity error is lower than 2.5%

Table 6.1 MCP performance

Quantity	Symbol	Value
Supply voltage	$\pm V_{DD}$	$\pm$ 5 V
Maximum drive voltage	$v_{a,\max}$	85 V
Test frequency	f_0	1 MHz
Maximum device frequency	$f_{r,\max}$	100 kHz
Resolution	$\sigma_{v,\text{out}}$	1 aF/$\sqrt{\text{Hz}}$[a]
Sensitivity	S	1.691 mV/fF[a]
Linearity	ε (%)	< 1
Temperature drift	$\Delta v_{\text{out}}/(v_{\text{out}} \cdot \Delta T)$	< 100 ppm/°C

[a]Measured at $v_0 = 450$ mV

into account the presence of the socket parasitic in the conversion between the output voltage and the measured capacitance. The evaluated average sensitivity is:

$$S = \frac{1.879\ \text{mV}_{\text{rms}}}{\text{V}_{\text{pp}} \cdot\ \text{fF}}\ , \tag{6.6}$$

with a good linearity error which is lower than 2.5%. Table 6.1 summarizes the performance of the MCP.

6.4 Industrialization of the Instrument

In order to transform the presented MCP prototype into a complete product, two blocks need to be further developed: (1) *on-board waveform generators*: both the test signal v_0 and the driving voltage v_d are, in the presented prototype, provided by an external voltage source or waveform generator. The aim is to replace them by using integrated components that allow to generate ramp, sine and square waves with controllable frequency and amplitude; (2) *power supply*: general purpose laboratory power supplies must be replaced by dedicated power supplies.

At the time of publication of this manuscript a product has already been developed with features and specifications reported in [20]. From the technical point of view, as the capacitive M/NEMS developed for scientific and industrial applications have an extremely variable range in terms of rest capacitance, capacitance variation, resonance frequency, air gap, and stiffness (thus pull-in voltage), the versatility of the MCP can be further increased. This can be accomplished through an increase of the maximum measurable motional frequency. It has been shown in Sect. 6.2 how the maximum detectable motion frequency $f_{r,\max}$ is related to the test signal frequency f_0. The improvement thus turns into an increase of the test frequency f_0, which affects and thus involves all the readout chain. Operational amplifier with a larger gain bandwidth product and still a low input-referred noise are required. For what concerns the rectifying stages, diodes in the configuration shown in Fig. 6.5 give a good rectifying up to few tens of MHz. The next-future target is thus to reach 20–50 MHz of maximum test signal frequency with the same readout scheme. Beyond these values, other demodulation schemes would be required (for instance, based on mixers). Note that an increase in the modulation frequency by a factor n also determines an increase in the signal amplitude by the same factor: this means that one can reach a higher SNR, or can keep the same SNR but with a lower electrostatic force applied during readout. This becomes extremely important for nanoelectromechanical systems, where reduced air gap and elastic stiffness can increase the device sensitivity to electrostatic forces and thus make the pull-in voltage very low.

References

1. Z. Izham, M.C.L. Ward, Sens. Actuators, A **115**(2–3), 392 (2004). doi:10.1016/j.sna.2004.04.055. http://www.sciencedirect.com/science/article/pii/S0924424704003358; The 17th European Conference on Solid-State Transducers
2. D. Horsley, in *Handbook of Silicon Based MEMS Materials and Technologies*, chap. 17 (Elsevier, Amsterdam, 2010)
3. G. Langfelder, A. Tocchio, M. Thompson, G. Jaramillo, D. Horsley, in *2010 IEEE Sensors* (2010), pp. 1765–1769. doi:10.1109/ICSENS.2010.5689961
4. C.C. Nguyen, R. Howe, IEEE J. Solid State Circuits **34**(4), 440 (1999). doi:10.1109/4.753677
5. E. Colinet, J. Juillard, L. Nicu, C. Bergaud, IEEE Trans. Instrum. Meas. **54**(4), 1438 (2005). doi:10.1109/TIM.2005.851054

6. J.J. Ruan, N. Monnereau, D. Trémouilles, N. Mauran, F. Coccetti, N. Nolhier, R. Plana, IEEE Trans. Instrum. Meas. **61**(2), 456–461 (2012). doi:10.1109/TIM.2011.2161937
7. G. Langfelder, A. Longoni, F. Zaraga, Sens. Actuators A **159**(2), 233 (2010). doi:10.1016/j.sna.2010.03.011. http://www.sciencedirect.com/science/article/pii/S0924424710001147
8. A. Technologies, Datasheet. http://www.home.agilent.com/agilent/redirector.jspx?action=obs&nid=-34124.3.00&lc=ita&cc=IT&ckey=776077&pubno=5989-4435EN&ltype=LitStation&ctype=AGILENT_EDITORIAL
9. QuadTech, Technical Datasheet. http://www.quadtech.com
10. Polytec Inc., Technical Datasheet. http://www.polytec.com/int/_files/LM_DS_PMA-400_2004_09_E.pdf
11. C. Rembe, R. Kant, R. Muller, in *Proceedings of SPIE*, vol. 4400 (2001), pp. 127–137
12. S. Firebaugh, J. Charles, H.K., R. Edwards, A. Keeney, S. Wilderson, IEEE Trans. Instrum. Meas. **53**(4), 1047 (2004). doi:10.1109/TIM.2004.831504
13. G. Langfelder, A. Longoni, A. Tocchio, E. Lasalandra, IEEE Sensors J. **11**(4), 1069 (2011). doi:10.1109/JSEN.2010.2078499
14. M. Thompson, M. Li, D. Horsley, in *2011 IEEE 24th International Conference on Micro Electro Mechanical Systems (MEMS)* (2011), pp. 593–596. doi:10.1109/MEMSYS.2011.5734494
15. C. Comi, A. Corigliano, G. Langfelder, A. Longoni, A. Tocchio, B. Simoni, J. Microelectromech. Syst. **19**(5), 1140 (2010). doi:10.1109/JMEMS.2010.2067437
16. X. Xiong, Y.L. Wu, W.B. Jone, IEEE Trans. Instrum. Meas. **54**(5), 1739 (2005). doi:10.1109/TIM.2005.855094
17. G. Nielson, G. Barbastathis, J. Microelectromech. Syst. **15**(4), 811 (2006). doi:10.1109/JMEMS.2006.879121
18. M. Lemkin, B. Boser, IEEE J. Solid State Circuits **34**(4), 456 (1999). doi:10.1109/4.753678
19. G. Langfelder, A. Longoni, F. Zaraga, Sens. Actuators, A **148**(2), 401 (2008). doi:10.1016/j.sna.2008.09.011. http://www.sciencedirect.com/science/article/pii/S0924424708004755
20. N. Aresi, *MEMS Characterization Platform*. ITmems S.r.l. Spin-off of Politecnico di Milano (2014). http://www.itmems.it/MCP_rev0.3_web.pdf